JACS
JOURNAL OF THE AMERICAN CHEMICAL SOCIETY
Article
pubs.acs.org/JACS

Populated Intermediates in the Thermal Unfolding of the Human Telomeric Quadruplex

Robert D. Gray, Robert Buscaglia, and Jonathan B. Chaires*

James Graham Brown Cancer Center, University of Louisville, Louisville, Kentucky 40202, United States

Supporting Information

ABSTRACT: Thermal denaturation profiles of several model oligonucleotides of the human telomere DNA sequence including d[A(GGGTTA)$_3$GGG] (Tel22) were determined using circular dichroism (CD), fluorescence of adenine → 2-aminopurine analogs, and fluorescence resonance energy transfer (FRET) to monitor the unfolding process at specific locations within the quadruplex. The resulting optical spectra vs temperature data matrices were analyzed by singular value decomposition (SVD) to ascertain the minimum number of species required to reproduce the unfolding spectral profiles. Global nonlinear least-squares fitting of the SVD amplitude vectors was used to estimate thermodynamic parameters and optical spectra of all species for a series of unfolding mechanisms that included one-, two-, and three-step sequential pathways F ⇌ I$_n$ ⇌ U, n = 0, 1, or 2) as well as two mechanisms with spectroscopically distinct starting structures (F$_1$ and F$_2$). The CD and FRET data for Tel22 unfolding between 4 and 94 °C in 25 mM KCl were best described by a sequential unfolding model with two intermediates, while the 2-aminopurine analogs required one intermediate. The higher melting intermediate I$_2$ had a transition midpoint temperature (T_m) of 61 °C and a CD spectrum with a maximum and minimum at ∼265 and ∼245 nm, respectively. The fluorescence emission spectra of the 2-aminopurine and FRET derivatives suggest greater solvent exposure of the 5′-AGGGTTA- segment in the intermediate compared to the folded state. The spectroscopic properties of the 61 °C intermediate suggest that it may be a triple helical structure.

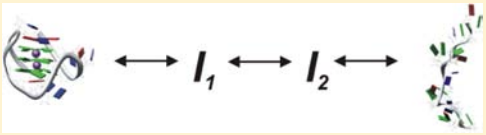

INTRODUCTION

Telomeres are supramolecular structures consisting of repetitive DNA sequences situated at the ends of chromosomes that function in maintaining chromosomal integrity and preventing loss of genetic information during cell division.[1] The human telomere consists of consecutive repeats of the DNA sequence d[GGGTTA]$_n$, 100−200 nucleotides of which are present in a single-stranded state at the 3′ end of the chromosomal DNA.[2−4] Normal cells are unable to fully replicate telomeric DNA during mitosis because of low levels of the enzyme telomerase, which is essential for telomere replication. Thus, as the telomeric sequence erodes during mitosis, the number n of hexanucleotide repeats decreases with the cellular age. This erosion triggers apoptosis, and the cell self-destructs. Cancer cells frequently have elevated telomerase levels and hence overcome telomere-dependent cell death.[5]

Single-stranded telomeric DNA sequences generally do not form classical double helical structures but instead undergo cation-dependent folding into a variety topologies that commonly consist of stacks of planar G-quartets connected by loops. The G-quartets themselves are stabilized by Hoogsteen-type H-bonds, while the quadruplexes form stacked G-quartets stabilized by monovalent cation coordination to the guanine O6 atoms. The loop sequences connecting stacked quartets determine the overall topography (tertiary structure or "fold") of the quadruplex. The topological complexity of G-quadruplex folding is more reminiscent of RNA and protein folding than of duplex formation.

NMR and X-ray crystallography have defined at least five topologies for human telomeric quadruplexes.[6] These topologies are characterized by the relative direction of the strand segments (parallel or antiparallel), the geometry of the connecting loops (diagonal, lateral, or chain reversal), and the size of the grooves that define the external surface (wide, narrow or medium). Since only relatively small energetic differences exist between different topologies, the predominant arrangement depends on the number of stacked quartets, the loop sequences, the identity of the coordinating cation, and the presence of 5′ or 3′ flanking residues. Monomolecular topologies that have been identified include: basket (antiparallel), chair (antiparallel), mixed (three antiparallel and one parallel), and all-parallel.

It is important to understand the thermodynamic factors that influence the relative stability of different conformers because this information is essential to understand the structure of the telomere and how switching between conformers could allow for regulation of telomere replication and to develop reagents that bind specifically to different conformers for use as drugs or structural probes.

Measurement of UV absorbance at a single wavelength is commonly used to monitor G-quadruplex thermal unfolding followed by analysis using a simple two-state model to extract thermodynamic parameters.[7−9] Representative thermodynamic parameters obtained by such methods have been tabulated and

Received: July 31, 2012
Published: September 18, 2012

dx.doi.org/10.1021/ja307543z | J. Am. Chem. Soc. 2012, 134, 16834−16844

discussed in recent reviews.[10,11] However, use of the two-state model may mask complexity in the denaturation process and therefore must be justified by experimental tests. Indeed, a study using calorimetry and circular dichroism (CD) to monitor human telomeric quadruplex denaturation showed that at least one stable intermediate state exists along the unfolding pathway.[12] A more recent study confirmed the existence of the intermediate state and provided a more sophisticated thermodynamic analysis of the process.[13]

Many unanswered questions remain about the mechanism of quadruplex denaturation, most importantly the number and nature of intermediate states along the unfolding pathway. Sugiyama and colleagues[14] used molecular dynamics simulations to explore possible folding pathways and proposed the existence of stable triple-helical intermediate states. Such states have yet to be identified and validated experimentally.

We undertook the current study as part of an overall goal to define the quadruplex energetic and kinetic landscapes using different spectroscopic probes to monitor the unfolding process in a site-specific manner to detect the presence of intermediates and to characterize their spectroscopic signatures to gain clues as to their structures. Here we use multiwavelength CD, fluorescence emission, and FRET spectroscopies to map the thermal unfolding pathway of a human telomeric model oligonucleotide, the 22-mer d[A(GGGTTA)$_3$GGG] (Tel22) in KCl solutions. All of the spectroscopic techniques revealed at least one intermediate structure which predominated at 55−60 °C for Tel22 as well as a variety of similar quadruplex-forming sequences. The CD and fluorescence properties suggest that this structure has properties expected of a triplex structure that has been suggested as an intermediate in the cation-driven folding of quadruplexes.

MATERIALS AND METHODS

Oligonucleotides. The sequences and code names of the oligonucleotides used in this study are given in Table 1. All oligonucleotides except for the FRET derivative 6-Fam-Tel22-Tamra were obtained in desalted, lyophilized form from Integrated DNA Technologies, Inc., Coralville, IA. They were dissolved in 10 mm tetrabutylammonium phosphate, 1 mM EDTA, pH 7.0 (folding buffer) at a concentration of 0.5−1 mM, and stored at 4 °C. The FRET oligonucleotide 6-Fam-Tel22-Tamra was obtained in HPLC-purified form from Sigma-Aldrich, St. Louis, MO. It was dissolved in folding buffer at a concentration of 250 μM and stored in an opaque container at 4 °C. Oligonucleotide concentrations were estimated from their absorbance at 260 nm using extinction coefficients supplied by the manufacturer. Other reagents were from Sigma-Aldrich.

Table 1. Sequences and Codes Names of the Oligonucleotides Used in This Study

oligonucleotide	sequence
Tel22	d[AGGGTTAGGGTTAGGGTTAGGG]
Tel22-AP1	d[2-ApGGGTTAGGGTTAGGGTTAGGG]
Tel22-AP7	d[AGGGTT2-ApGGGTTAGGGTTAGGG]
Tel22-AP13	d[AGGGTTAGGGTT2-ApGGGTTAGGG]
Tel22-AP19	d[AGGGTTAGGGTTAGGGTT2-ApGGG]
2GKU[a]	d[TTGGGTTAGGGTTAGGGTTAGGGA]
2AQY[a] + 6	d[GGGTTAGGGTTAGGGT] + d[TAGGGT]
Tel-3G	d[TTAGGGTTAGGGTTAGGGTTA]
6Fam-Tel22-Tamra	6-Fam-d[AGGGTTAGGGTTAGGGTTAGGG]-Tamra

[a]PDB designation for the structure.[38,39]

Thermal Denaturation Experiments. Thermally induced quadruplex unfolding was followed either by CD or by fluorescence emission essentially as described previously.[15] Duplicate melts were carried out on the same sample on successive days; all results reported here are for the second melt. A third melt on the same sample generally gave results that were identical to the second melt.

For CD experiments, samples were prepared by dilution of a concentrated stock solution of oligonucleotide at a previously determined concentration into folding buffer. Reference CD and absorbance spectra were recorded in a stoppered 1 cm path length cuvette at 20 °C with a Jasco J-810 spectropolarimeter equipped with a programmable Peltier thermostat and a magnetic stirrer. The desired salt concentration was then established (generally 25 mM KCl or 100 mM NaCl) by adding the requisite volume of 3 M salt solution. The instrumental parameters for the CD melting experiments were: 1.0 nm bandwidth, 2 s integration time, 200 nm/min scan rate, 4 °C/min ramp, ±0.05 °C equilibration tolerance, 60 s delay after equilibration. Three spectra were averaged at each temperature. CD data were normalized to strand concentration using the equation $\varepsilon_L - \varepsilon_R = \Delta\varepsilon = \theta/(32\,980 \cdot c \cdot l)$, where θ is the observed ellipticity in millidegrees, c is the DNA strand concentration in mol·L^{-1}, and l is the path length in cm.

Fluorescence melting profiles were obtained using 1 cm path length stopped fluorescence cuvettes in a Jasco FP-6500 fluorometer equipped with a programmable Peltier thermostat and a magnetic stirrer. Sample preparation was the same as described for the CD melts. Instrumental operating parameters were: 5 nm excitation and 10 nm emission bandwidths for 2-AP derivatives and 5 nm/5 nm bandwidths for 6-Fam FRET experiments, 1 °C/min ramp, ±0.2 °C equilibration tolerance, 60 s delay after equilibration. Two spectra were averaged at each temperature. Excitation was at 305 or 490 nm for 2AP or 6-Fam FRET samples, respectively. Fluorescence and CD spectra were corrected by subtracting a blank (buffer only) spectrum.

Data Analysis by SVD. The CD or emission spectra obtained as a function of temperature T were assembled into a data matrix $\mathbf{D}_{i,j}$ consisting of i rows of spectroscopic signal (e.g., CD or fluorescence intensity) at wavelengths λ_i over in 1 or 2 °C increments from 4 to 94 °C unless otherwise noted. In $\mathbf{D}_{i,j}$, row i represents a melting profile at λ_i, and column j represents the optical spectrum at T_j. $\mathbf{D}_{i,j}$ were analyzed by singular value decomposition (SVD) as previously described[15] to produce the **S**, **U**, and **V** matrices. **S** contains the singular values (the weights of the components comprising the data set), **U** contains the basis spectra (the spectral shapes) that make up the data set, and **V** contains the amplitudes of each component as a function of the experimental variable (temperature). SVD was carried out using the matrix algebra routines in the software suite Mathmatica 8.0 (Wolfram Research, Champaign, Il). The number of significant spectral components contained in $\mathbf{D}_{i,j}$ was determined by evaluating the relative magnitude of the singular values, their contribution to the total variance of the signal, and the values of the autocorrelation coefficients of the amplitude (**V**) vectors.

Mechanistic Analysis of Thermal Unfolding Data. Since the SVD analysis generally showed evidence for at least three spectroscopically distinct species over the experimental temperature range, we considered five pathways shown in in Scheme 1 that might reasonably describe the temperature-dependent stability of quadruplex DNA. To analyze the data in terms of these mechanisms, the significant **V** vectors (defined as those vectors with autocorrelation coefficients ≥0.75) were globally fit by iterative nonlinear least-squares to the analytical expressions for thermal unfolding corresponding to each mechanism. These equations, which are based on van't Hoff analysis of multiple thermal transitions, were either taken from the literature[16,17] or derived specifically for this study; they are summarized in Figure S1, Supporting Information.

In brief, the spectral signal associated with each pure species in the mechanism (e.g F, I$_n$, and U) as well as the respective van't Hoff enthalpies ΔH and transition midpoint temperatures (T_m) for each were optimized by iterative nonlinear least-squares analysis using routines programmed in Mathmatica 8.0. The species designated F, I, and U most likely consist of ensembles of energetically equivalent

Scheme 1. Mechanisms Describing Thermal Unfolding of G-Quadruplexes

1) $F \rightleftharpoons U$

2) $F_1 \rightleftharpoons U \rightleftharpoons F_2$

3) $F \rightleftharpoons I \rightleftharpoons U$

4) $F \rightleftharpoons I_1 \rightleftharpoons I_2 \rightleftharpoons U$

5) $F_1 \rightleftharpoons I \rightleftharpoons U$, with $I \updownarrow F_2$

F = folded state(s)
I = intermediate state(s)
U = unfolded ensemble

conformers rather than a specific conformation. Fits to the individual mechanisms were compared by their respective χ^2 values and residual plots. Uncertainties of the fitted parameters were derived by carrying out 1000 Monte Carlo simulations as described by Saroff.[18] Models with different numbers of adjustable parameters were compared using the Akaike information criterion (AIC) statistical analysis to account for the increased degrees of freedom associated with an increase in adjustable parameters.[19]

RESULTS

Melting of Tel22 Assessed by CD. We initially utilized temperature-dependent CD to investigate the unfolding pathway of Tel22 in 25 mM KCl. CD spectroscopy is sensitive to topological features of nucleic acid structure, particularly the orientation of guanine bases within the G-quartet stack. A family of spectra associated with a representative melt is shown in Figure 1A. The spectra of the folded state F at 4 °C have a maximum at ∼289 nm and a minimum at ∼235 nm with a prominent shoulder at ∼270 nm. This spectrum is characteristic of a mixture of quadruplex conformers suggested by biophysical studies of this sequence in K^+-containing solutions.[20−22] As the temperature was increased, a new species appeared which has a maximum in the CD spectrum near 266 nm and a minimum near 242 nm; this signal is maximal at ∼65 °C. The 266 nm species subsequently decayed to the unfolded state U as the temperature was increased to 94 °C. The unfolded ensemble has a relatively weak CD spectrum characteristic of a disordered polynucleotide.

A hallmark of a multistate denaturation process is that the progress unfolding curves measured at different wavelengths or determined with different spectral techniques differ.[23,24] This complexity is evident in Figure 1B which shows the temperature variation of the CD signal at 290 and 265 nm. The differences between the two melting profiles can be readily appreciated by comparing the first derivative curves: The inflection points in the derivative curves indicate the number of melting events as well as the midpoint temperature associated with each. As shown in Figure 1B, bottom panel, the 290 nm data exhibit a minimum at 50 °C, while the 265 nm data have a maximum at 46 °C and a minimum at 64 °C. From this, we conclude that the thermal unfolding pathway of Tel22 in 25 mM KCl cannot be described by the two-state pathway 1 in Scheme 1 but rather requires a more complex pathway. The three distinct inflection temperatures suggest contributions to the melting curves from at least four species as in mechanisms 4 and 5 in Scheme 1.

A rigorous procedure for determining the minimum number of spectroscopically distinct species in the unfolding experiments is to perform SVD on data sets that include all temperature-dependent spectra and then compare the singular values and the dependence of the **V** vectors (the amplitudes of each component) on temperature. The results of an SVD analysis of the data set in Figure 1A are summarized in Figure 2, which shows the temperature dependence of the four highest ranking **V** vectors ($\mathbf{V}_1 - \mathbf{V}_4$) and in Table 2, which summarizes the results of the analysis.

The SVD analysis suggests that at least three and possibly four species contribute significantly to the CD spectrum of Tel22 over the temperature range 4−94 °C. In Table 2, the three species with the highest singular values contribute 99.88% of the total variance. In addition, these species have **V** autocorrelation coefficients >0.9, showing the systematic variation in the amplitude vectors with temperature. Figure 2A,B shows that the four most significant amplitude vectors have temperature-dependent inflections as reflected in the relatively high values for their autocorrelation coefficients. The autocorrelation coefficient for $\mathbf{V}_4$ (0.78) was slightly less than

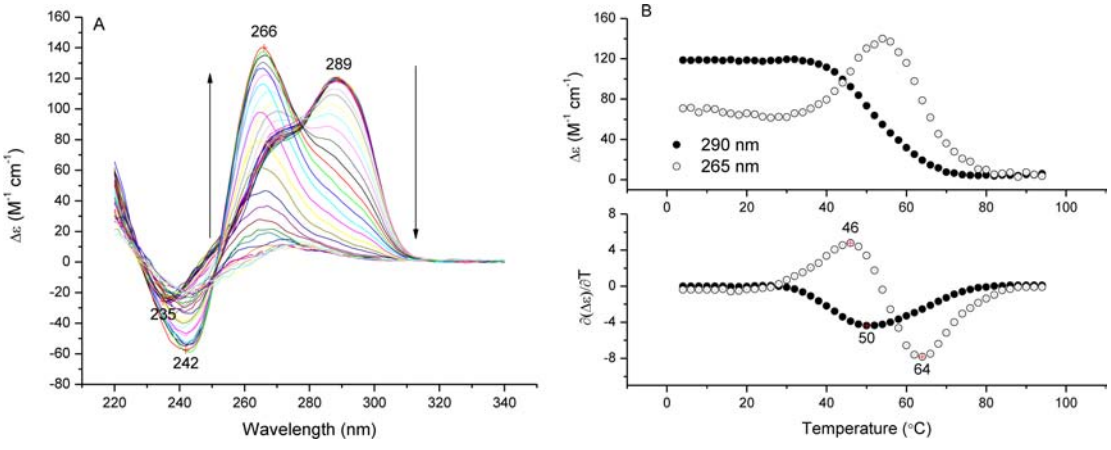

Figure 1. Temperature-dependent unfolding of Tel22 in 25 mM KCl as assessed by CD. (A) Family of CD spectra of Tel22 in 25 mM KCl as a function of temperature from 4 to 94 °C measured as described in Materials and Methods section. The arrows indicate the direction of the temperature change. (B, top panel) Single wavelength melting curves showing temperature dependence of the CD signal at 290 and 265 nm taken from the spectra of (A). (B, bottom panel) First derivative of the data in (B). The inflection points in the derivative curves (annotated in the figure) approximate the T_m values for the two processes.

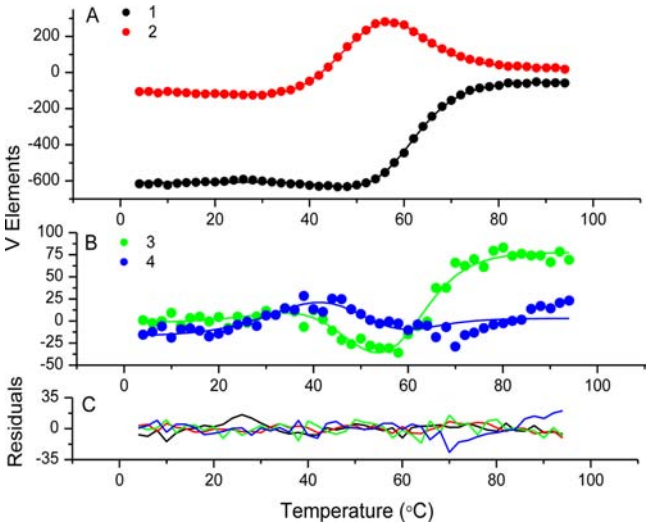

Figure 2. SVD analysis of thermal unfolding of Tel22 in 25 mM KCl. (A) Thermal profiles of vectors $\mathbf{V}_1$ and $\mathbf{V}_2$. (B) Profiles for $\mathbf{V}_3$ and $\mathbf{V}_4$ derived from the data set in Figure 1A. The lines illustrate the least-squares fit of the data points to the three-step sequential mechanism 4 in Scheme 1. (C) Residual plots for the fits to the four vectors. The optimized parameters and the fitting equation are summarized in Table 3 and in Supporting Information.

Table 2. Parameters from SVD Analysis of Melting Data for Tel22 in Figure 1A

index	singular value	% of total variance	V matrix autocorrelation coefficient
1	3303.96	92.30	0.9811
2	905.37	6.93	0.9789
3	278.22	0.65	0.9312
4	91.06	0.07	0.7774
5	37.28	0.01	−0.2056

0.8, a value generally taken as a cutoff value for significance.[25] However, as described in the next section, including $\mathbf{V}_4$ in the global least-squares analysis resulted in a significantly better fit of the data to a four species pathway compared to a three species pathway. This improvement in the quality of the fit led us to include $\mathbf{V}_4$ in the least-squares analysis of the data.

Assignment of Thermal Unfolding Pathway for Tel22 in KCl Based on CD Melting. Table 3 summarizes the statistics obtained by least-squares fitting of the data set corresponding to the melt in Figure 1A to the analytical expressions corresponding to the mechanisms in Scheme 1. It is clear from the χ^2 statistics that models 1−3 are inferior representations of the data, whereas models 4 and 5 (each with four species) give equally good fits by this criterion. The decreased AIC values for models 4 and 5 indicate that the enhanced fit with four rather than three species cannot be attributed to the increased number of adjustable parameters in the four-species model.

Table 3. Model-Dependent Fitting Statistics for Thermal Unfolding of Tel22 in 25 mM KCl Monitored by CD

model	model	χ^2	AIC value
single transition	1	720265.5	1544.1
two transitions	2	15235.4	846.6
parallel transitions	3	15235.4	846.6
three transitions	4	7759.5	734.5
parallel intermediate transitions	5	7757.3	734.4

Since both models 4 and 5 gave equally good fits, we looked for another means to distinguish between them. To accomplish this we used the optimized values of the fitted thermodynamic parameters in Table 4 to estimate the standard free energy change ΔG for each species at 20 °C. We reasoned that the sequential, two-intermediate model 4 is consistent with the supposition that Tel22 in KCl is a mixture of at least two conformers present in roughly equal amounts.[20,21,26] Thus, the two structures must have approximately the same Gibbs free energy of folding. The calculated $\Delta\Delta G$ of 1.7 kcal mol^{-1} for the two conformers in model 5 requires an F1:F2 ratio of approximately $e^{-1.7/RT} \approx 22.5{:}1$, which is clearly larger than the expected 1:1 ratio.

Table 4. Optimal Values of Thermodynamic Parameters for Folding Tel22 in 25 mM KCl[a]

	model 4	model 5
ΔH_1	−21.9 ± 4.7[b]	−25.3
T_{m_1}	35.2 ± 5.3	48.4
ΔH_2	−33.4 ± 4.2	−54.6
T_{m_2}	47.6 ± 1.6	42.8
ΔH_3	−45.3 ± 4.2	−43.6
T_{m_3}	61.4 ± 1.0	60.7
ΔG_1	−1.1 ± 0.4	−2.2
ΔG_2	−2.9 ± 0.4	−3.9
ΔG_3	−5.6 ± 0.6	−5.3
ΔG_{Total}	−9.5 ± 0.7	−11.5

[a] ΔH and ΔG values are in kcal mol^{-1}, and T_m values are in °C. Standard free energy changes ΔG are calculated for 20 °C. [b] Standard deviations derived from 1000 Monte Carlo simulations.[18]

CD Spectra of Intermediates in the Thermal Unfolding of Tel22 in KCl. Fitting a CD data matrix to an explicit unfolding mechanism allows calculation of the spectra of each of the significant species as well as their relative distributions along the unfolding pathway.[15,25] The calculated spectra and species distribution plots associated with model 4 are shown in Figure 3.

The spectra of the folded and unfolded ensembles obviously are very similar to the low- and high-temperature spectra in Figure 1A. The spectrum of I_1 resembles that of a folded quadruplex.[27] The spectrum of I_2 resembles that of Tel22 in KCl−acetonitrile, which is thought to be the all-parallel form.[28] The CD spectra the all-parallel form and the intermediate I_2 have a maximum at ∼265 nm and a minimum at ∼245 nm. However, the intensity ($\Delta\varepsilon$) of the 265 nm peak for I_2 is about three-fourths of that for the all-parallel form, suggesting that I_2 is not in the all-parallel state. In addition, as shown below for fluorescent analogs of Tel22 which form a similar intermediate at 55−65 °C, the fluorescence properties of the intermediate are inconsistent with those expected for the parallel conformation.

Melting of 2-AP Derivatives of Tel22 Assessed by Fluorescence Quantum Yield. To further characterize the intermediate state(s) of Tel22, we determined the melting profiles of fluorescent derivatives of Tel22. 2-Aminopurine (2-AP) is a fluorescent analog of adenine whose fluorescence quantum yield is sensitive to various environmental and structural factors.[29−32] Serial substitution of 2-AP for the 5′

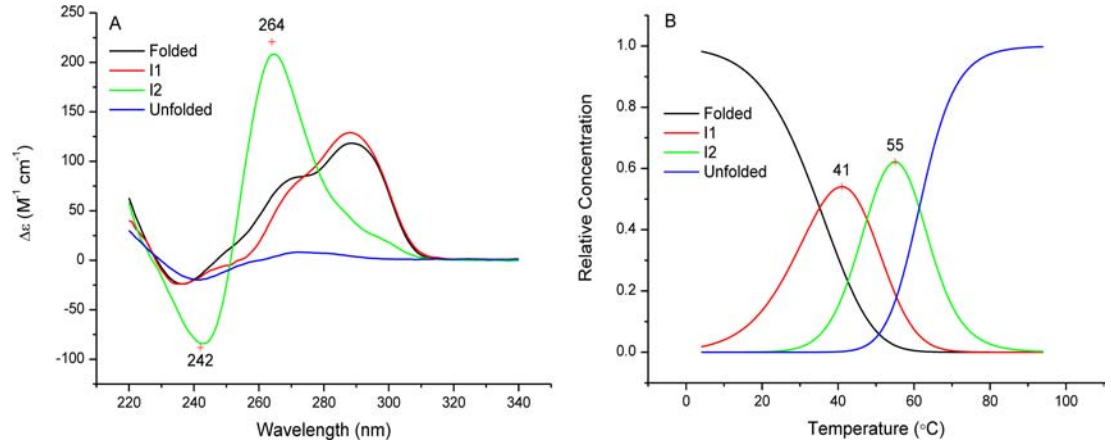

Figure 3. Calculated CD spectra and relative concentration profiles for the species derived by SVD analysis and fitting the data set in Figure 1A to the analytical expression associated with the sequential intermediate model 4. (A) CD spectrum of each significant species. (B) Relative concentrations of each as a function of temperature.

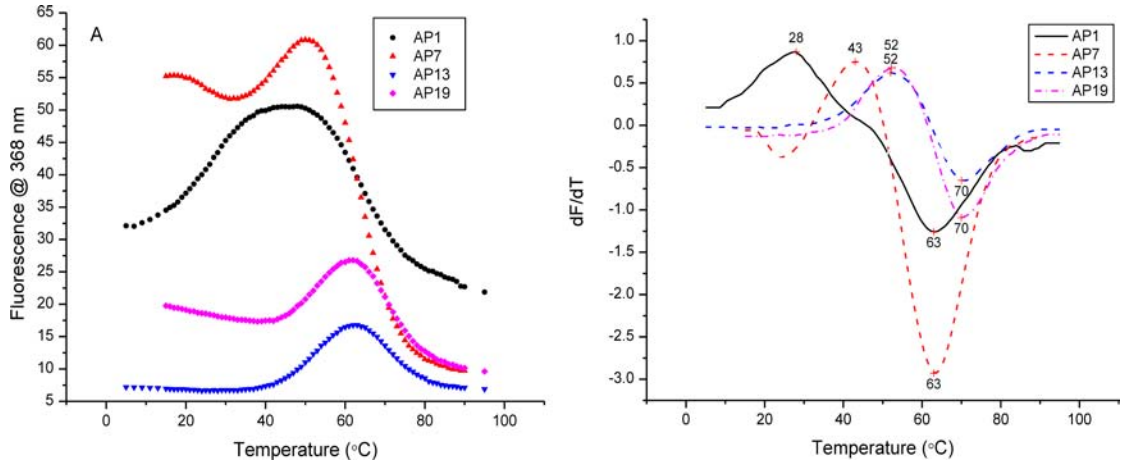

Figure 4. (A) Melting profiles for the temperature dependence of the emission intensity of the derivatives of Tel22 in which each of the four A residues is substituted serially with 2-AP. The numbers in the legend on the figures show the position of the 2-AP substitution in the sequence of Tel22. (B) First derivative curves of the data in (A). The numbers in (B) give the temperature associated with the maxima or minima in the curves. These temperatures are the approximate T_m of each step in the melting thermally induced unfolding process.

terminal A and for the three-loop A residues provides a sensitive reporter of the local environment at these positions and thus potentially could indicate changes in loop geometry during melting independently of G-quartet melting.[33,34] Previous studies from our laboratory have shown that A → 2-AP substitutions do not grossly perturb the structure of Tel22 in Na^+ or K^+ solutions as assessed by T_m or CD and therefore can be used to track folding as a function of cation concentration without perturbing the structure.[22,35] In addition, the quantum yield,[35] excited-state lifetimes,[34] and accessibility of the 2-AP analogs of Tel22 to collisional quenchers, such as acrylamide, depends on the position of the 2-AP residue within the sequence. Thus we expect that the melting profiles of the four different 2-AP derivatives of Tel22 assessed by changes in emission intensity may reveal intermediates during thermally induced unfolding.

The temperature-dependent emission spectra of Tel22 with position-specific A → 2-AP substitutions are given in Figures S2−S5. As expected, the emission maxima were invariant with temperature. However, a multiphasic response of emission intensity with respect to increasing temperature was noted for all four of the 2-AP derivatives of Tel22 (Figure 4A). The derivative spectra in Figure 4B reveal that the loop variants AP7, AP13, and AP19 have inflections in their first derivative curves in temperature ranges of 43−52 and 64−70 °C, while the terminal AP1 has inflections at 28 and 63 °C. The multiple inflections in the first derivative curves show that the changes in 2-AP emission intensity track at least three states during the unfolding process. In contrast, the emission intensity of the Tel22 2-AP derivatives in the absence of KCl as well as that of a control oligonucleotide in 100 mM KCl (d[TT-2-AP-GT]) were only weakly temperature dependent (Figure S6). The sharp inflections seen in Figure 4 above ∼25 °C are therefore associated with quadruplex unfolding rather than temperature effects on the intrinsic emission properties of 2-AP.

SVD analysis of the fluorescence emission data sets (Figures S2−S5) for melting of the 2-AP derivatives of Tel22 shows that three species contribute 99.99% of the variance and that all three of these species exhibit **V** matrix autocorrelation coefficients >0.75 (Table 5). Based on autocorrelation, the fluorescence studies with 2-AP-Tel22 are consistent with model 3 in which three species (F, I, and U) are populated in thermal unfolding of Tel22. Although the AIC statistic suggests an improved fit with more species, the low value of the

dx.doi.org/10.1021/ja307543z | J. Am. Chem. Soc. 2012, 134, 16834−16844

Table 5. Model-Dependent Fitting Statistics and SVD Analysis Results for 2-AP Derivatives of Tel22 Melting in 25 mm KCl

model selection statistics			SVD analysis statistics			
oligo/model	χ^2	AIC	index	singular value	% of total variance	**V** matrix autocorrelation coefficient
				AP1		
1	557 472.5	2461.7	1	3149.58	100.00	0.9940
2	404.2	102.6	2	16.14	0.00	0.9666
3	404.3	102.6	3	5.67	0.00	0.8438
4	104.6	−328.9	4	2.60	0.00	0.3781
5	194.6	−125.2	5	1.94	0.00	0.1318
				AP7		
1	37 090.4	1482.4	1	3483.35	100.00	0.9895
2	3437.8	771.4	2	16.84	0.00	0.9576
3	3445.9	772.1	3	6.82	0.00	0.8801
4	3437.8	783.4	4	3.86	0.00	0.1726
5	74.3	−382.2	5	3.01	0.00	0.1310
				AP13		
1	39 202.9	1591.0	1	820.25	99.96	0.9936
2	133.1	−261.9	2	16.58	0.04	0.9683
3	133.1	−261.9	3	1.83	0.00	0.4841
4	15.4	−956.3	4	1.43	0.00	−0.0361
5	15.4	−956.3	5	1.31	0.00	0.0156
				AP19		
1	44 883.5	1556.4	1	1503.22	99.98	0.9911
2	1763.8	571.5	2	23.25	0.02	0.9848
3	1763.8	571.5	3	3.17	0.00	0.8454
4	1763.8	583.5	4	1.72	0.00	0.0588
5	44 883.5	1580.4	5	1.62	0.00	0.1135

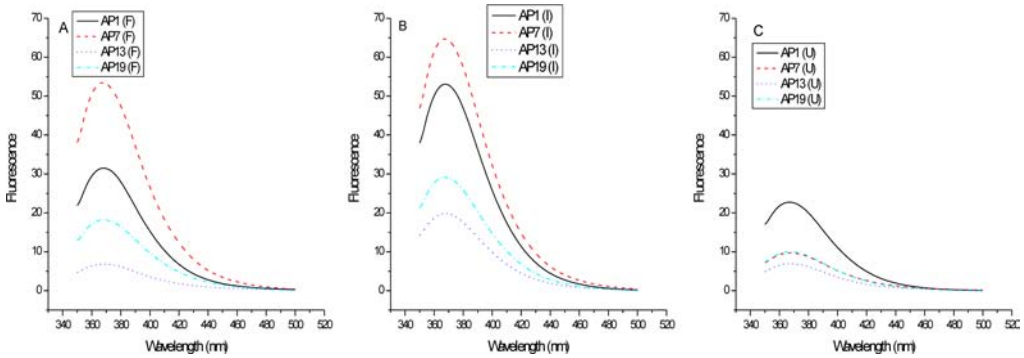

Figure 5. Emission spectra of 2-AP derivatives of Tel22 in 25 mM KCl determined by SVD analysis of the thermal unfolding of Tel22 with serial substitutions of 2-AP at each A residue. (A–C) Calculated spectra of the folded ensemble, the intermediate species, and unfolded ensemble, respectively. The spectra were calculated using model 2 and the optimized thermodynamic parameters in Table 6.

autocorrelation coefficients for $\mathbf{V}_4$ does not justify including a fourth species.

Emission Spectra and Thermodynamic Parameters for Melting of 2-AP Derivatives of Tel22. Fitting the 2-AP data matrices corresponding to the data of Figures S2–S5 to the analytical expression describing the two-step sequential mechanism allows determination of the emission spectra as well as the T_m and ΔH_{vH} for melting of the F and I ensembles. These spectra are collected in Figure 5, and the fitted parameters are in Table 6. Comparison of the spectra shows at all positions; the emission of the intermediate is enhanced compared to both the folded structures and the unfolded structures. Moreover, the emission intensity of the intermediate structures is clearly different with AP7 > AP1 > AP19 > AP13.

Fluorescence Melting of 6-Fam-Tel22-Tamra. An additional spectroscopic probe to aid in defining the thermal unfolding pathway is the FRET-labeled derivative of Tel22.

Table 6. Optimal Thermodynamic Parameters for Folding 2-AP Derivatives of Tel22 in 25 mm KCl Assuming Model 2[a]

	T_{m_1}	ΔH_1	T_{m_2}	ΔH_2	ΔG_1	ΔG_2	ΔG_{Total}
Tel22-AP1	26.5	−27.7	64.6	−37.0	−0.6	−4.9	−5.5
Tel22-AP7	45.4	−79.2	63.8	−49.1	−6.3	−6.4	−12.7
Tel22-AP13	53.6	−45.5	70.6	−51.9	−4.7	−7.6	−12.3
Tel22-AP19	54.1	−70.3	71.6	−53.9	−7.3	−8.1	−15.4

[a] ΔH and ΔG values are in kcal mol^{-1}and T_m values are in °C. Standard ΔG values are calculated for 20 °C.

Folding of such models of the human telomere sequence has been investigated using oligonucleotides with suitable donor and acceptor fluorophores, such as 6-carboxyfluorescein and

dx.doi.org/10.1021/ja307543z | J. Am. Chem. Soc. 2012, 134, 16834–16844

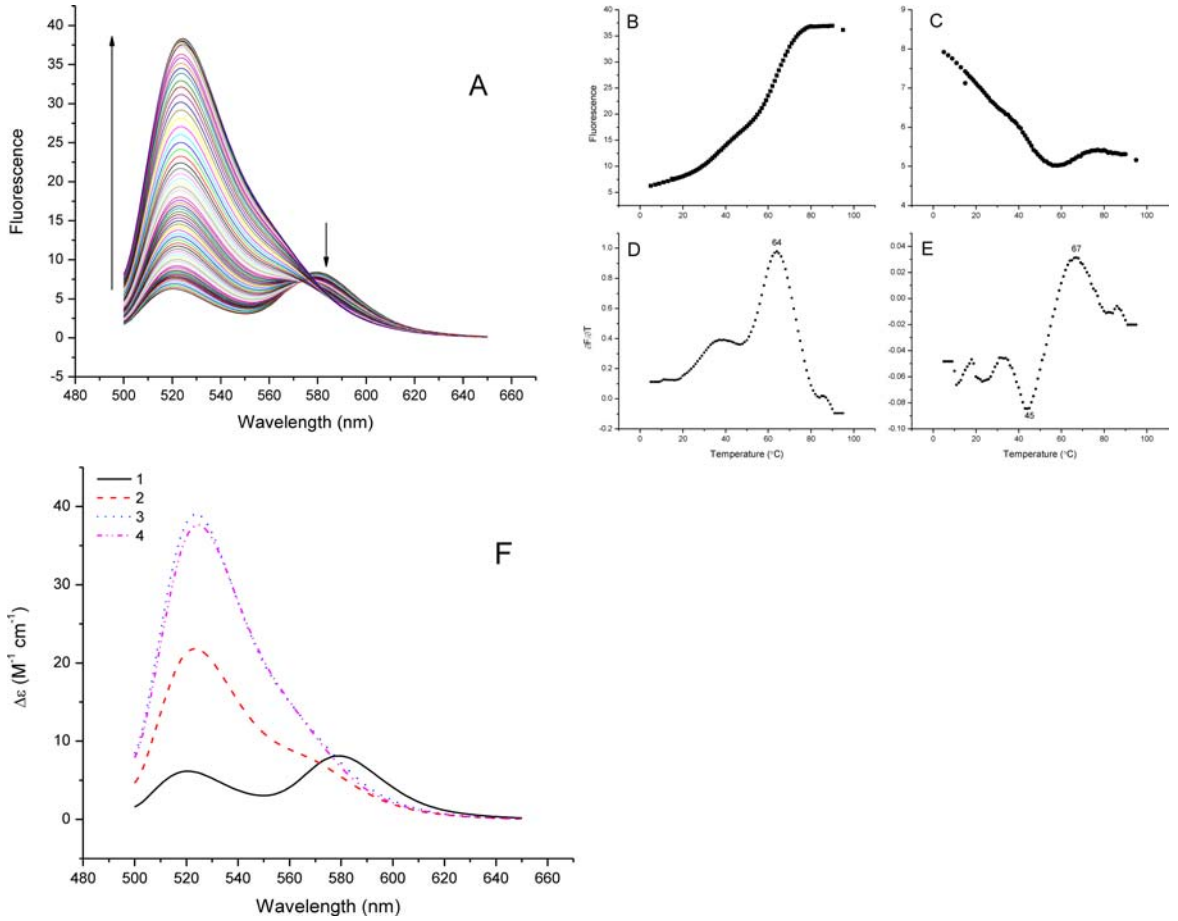

Figure 6. Thermal melting of 6-Fam-Tel22-Tamra in 25 mM KCl assessed by changes in FRET efficiency. (A) Family of emission spectra collected as a function of temperature between 5 and 95 °C. The arrows show the direction of the change (increase or decrease) in emission intensity with increasing temperature. (B,C) Changes in emission intensity at 520 nm (6-Fam) and 585 nm (Tamra) with increasing temperature derived from the spectra in (A). The first derivative spectra in (D,E) show at least two major inflections in the melting profiles at ∼45 and ∼65 °C. (F) Emission spectra of the four species obtained by fitting the data set to model 4 using the parameters in Table 7.

tetramethylrhodamine linked to the 5′ and 3′ ends of the oligonucleotide.[36,37] Since the termini of telomeric oligonucleotides are brought closer together during the folding process, folding should increase the efficiency of energy transfer, which would be apparent from quenching the 6-Fam fluorescence at 520 nm and enhancement of Tamra fluorescence at 585 nm. The oligonucleotide 6-Fam-Tel22-Tamra is expected to provide a sensitive test of the multistate folding process because appearance of a stable folding intermediate should manifest itself as a change in the distance and/or orientation properties of the FRET donor and acceptor which in turn will influence FRET efficiency.

Figure 6 illustrates the emission spectra of 6-Fam-Tel22-Tamra as a function of temperature in 25 mM KCl. Figure 6B,C shows the thermal unfolding profiles of 6-Fam-Tel22-Tamra at 520 and 585 nm, the emission maxima of 6Fam and Tamra, respectively. The intensity of the donor emission increases with temperature while that of acceptor concomitantly decreases as expected for an unfolding process which separates the donor and acceptor probes. The corresponding first derivative spectra $\partial F/\partial T$ (Figure 5D,E) reveal inflection points at ∼45 and 65 °C.

Analysis of the data set in Figure 6 by SVD shows that four species contribute 99.99% of the variance and that the **V**-profiles of the four species have autocorrelation coefficients >0.95 (Tables S1 and S2). Fitting the melting data to mechanism 4 resulted in the species emission spectra shown in Figure 6C and the thermodynamic parameters summarized in Table 7. We conclude that the FRET melting data are consistent with a multistep melting process for Tel22.

Melting of Quadruplex-Forming Oligonucleotides with Variant Sequences. An important question arising from characterization of thermal unfolding of Tel22 is whether the heterogeneous pathway is unique. Is the complexity a consequence of the known topological heterogeneity of the Tel22 system in KCl at room temperature? To answer this question, we investigated the thermal unfolding of a variety of quadruplex-forming oligonucleotides of known structure shown in Table 1. 2GKU was chosen because NMR shows that it forms predominantly a single structure (the so-called hybrid-1 fold) in KCl.[38] 2AQY, a 16-mer with three G_3 runs ($d[(G_3T_2A)_2G_3T]$), forms a quadruplex in 100 mM NaCl in the presence of a hexamer with a single G_3 run ($d[AG_3T]$)[39], and Tel-3G ($d[(T_2A(G_3T_2A)_3]$) has been reported to form a triplex in NaCl and KCl.[40] In each of these cases, we observed a multistep unfolding process (data in Figures S6−S8).

CD Spectra of the Intermediates Suggest a Common Structure. The CD spectra of the melting intermediates are compared in Figure 7, and the corresponding spectra of the folded and unfolded states are given in Figures S7−S9. The

dx.doi.org/10.1021/ja307543z | J. Am. Chem. Soc. 2012, 134, 16834−16844

Table 7. Thermodynamic Parameters for Folding 6-Fam-Tel22-Tamra and Quadruplex Forming Sequence Variants[a]

	model	T_{m_1}	ΔH_1	T_{m_2}	ΔH_2	T_{m_3}	ΔH_3	ΔG_1	ΔG_2	ΔG_3	ΔG_{Total}
6Fam-Tel22-Tamra	4	39.7	−18.5	65.1	−45.7	86.5	−45.9	−1.2	−6.1	−8.5	−15.8
2GKU	4	33.8 ± 6.6[b]	−21.1 ± 8.1	53.8 ± 1.9	−41.4 ± 6.2	60.8 ± 1.2	−55.8 ± 6.6	−0.9 ± 0.4	−4.3 ± 0.6	−6.8 ± 0.9	−12.0 ± 1.0
2AQY + 6	3	40.3	−36.0	57.9	−19.8	–	–	−2.3	−2.3	–	−4.6
Tel-3G	3	46.3	−19.8	70.4	−21.0	–	–	−1.6	−3.1	–	−4.7

[a] ΔH and ΔG values are in kcal mol^{-1}, and T_m values are in °C. Standard ΔG values are calculated for 20 °C. [b] Standard deviations derived from 1000 Monte Carlo simulations.[18]

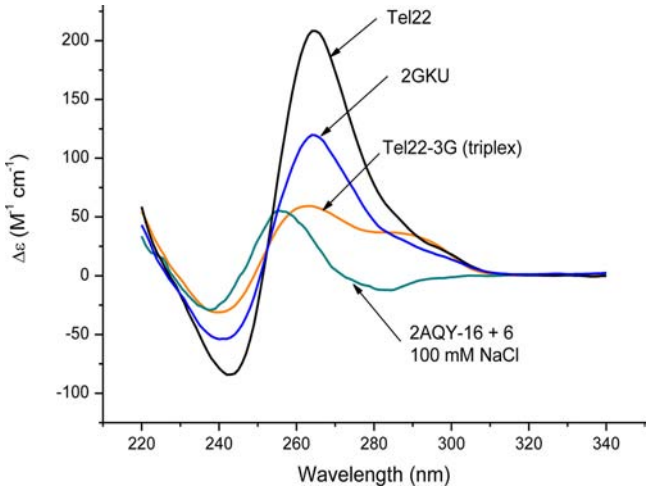

Figure 7. CD spectra of thermal unfolding intermediates derived by SVD analysis of the wavelength-dependent melting profiles and fitting the resulting significant **V** vectors of each data set to mechanism 3 or 4 in Scheme 1.

spectra of the intermediate state for Tel22 and 2GKU (Figure 7) are similar with maxima at ∼265 nm and minima at ∼244 nm. The 2AQY system has a spectrally similar intermediate whose maximum is shifted slightly to shorter wavelengths. The fourth spectrum in Figure 7 is that of a triplex-forming structure, Tel-3G. It is noteworthy that the spectral shape and the positions of the maximum and minimum of Tel-3G are similar to those of the quadruplex-forming oligonucleotides. These results show that similar intermediates are produced from both oligonucleotides and that the melting mechanism is not unique to Tel22.

The position and magnitude of the of the CD spectra of the intermediate resemble that of the all-parallel topography, which generally has a maximum in the vicinity of 265 nm and a smaller minimum near 245 nm.[27] However, an all parallel topography is not consistent with the emission spectra of the 2-AP and FRET analogues of Tel22 as discussed below.

■ DISCUSSION

We make four major points regarding the thermal unfolding of G-quadruplex forming oligonucleotides: (1) the thermal denaturation of quadruplex in KCl cannot be adequately described as a simple two-state unfolding process but rather requires three or four species to fit multiwavelength CD, fluorescence emission, or FRET spectral profiles over the temperature range of 4−90 °C; (2) the spectroscopic data support sequential mechanisms 3 and 4 outlined in Scheme 1; (3) the sequential pathway is common for two sequences (Tel22 and 2GKU) that exhibit differing degrees of structural heterogeneity at room temperature; and (4) taken together, the 2-AP fluorescence and FRET melting experiments are inconsistent with the hypothesis that the intermediate state is an all-parallel folded state. The spectral properties of the intermediate state melting at 55−65 °C are consistent with its identification as a triple-helical structure. Our results and conclusions apply only to the human telomere quadruplex which is known adopt a variety of structures. Whether other types of quadruplexes have multistate unfolding pathways is not known and requires investigation.

Implications of Multistate Melting. Published studies often have assumed that quadruplex melting follows a simple

two-state reaction in Scheme 1, thus allowing estimation of van't Hoff enthalpy changes and associated (derived) thermodynamic parameters, such as $\Delta G_{folding}$ from a single melting curve. This is in spite of the fact that numerous calorimetric studies have shown that some quadruplex thermograms derived by DSC require more than two species in equilibrium during the entire course of the melt.[12,13] The assumption of two-states should be justified by showing, for example, that monitoring unfolding at two or more wavelengths or by two independent methods gives overlapping results for the unfolding profile.[15,23,24,41,42] By these criteria, the unfolding of Tel22 in KCl and its sequence homologues are certainly not two-state. Without verification of the model, the derived thermodynamic parameters may be invalid.

What are the consequences of neglecting the complexity of the quadruplex unfolding mechanism? Analysis using single-wavelength data and the two-state assumption lead to underestimates of the thermodynamic parameters of the denaturation reaction and to possible misconceptions about quadruplex stability. This can be illustrated by using the data in Figure 1B. The melting curve obtained as recommended[9] at 295 nm appears to be consistent with a two-state process and can be fit to yield T_m = 52.6 and ΔH = 30.4 kcal mol^{-1} for the denaturation reaction, from which $\Delta G_{20°C}$ = −2.6 kcal mol^{-1} (for folding) can be obtained. These values are fully consistent with literature reports for the stability of this quadruplex.[11] But this free energy estimate is much smaller in magnitude than that obtained using the sequential mechanism demanded by our analysis (Table 4) and gives the erroneous impression of a less stable folded form. The origins of the problem may arise from (at least) two possible sources: First, by using a single wavelength to monitor quadruplex denaturation, one may focus on the melting of only a particular region of the molecule and miss the contributions of other regions to the unfolding process. Note that the thermodynamic parameters obtained by the two-state analysis using only the 295 nm data most closely resemble those that characterize the second step in the sequential mechanism, which we assign to the $I_1 \rightarrow I_2$ transition. Alternatively, a melting curve obtained at a single wavelength may not fully resolve into multiple transitions, appearing instead as a single broad transition. Since the van't Hoff enthalpy determines the slope and width of the transition, an underestimate of the true underlying overall enthalpy would result.

Reliable thermodynamic parameters are necessary for any attempt to predict quadruplex stability. Recently a novel Bayesian prediction framework based on Gaussian process regression was used to predict the thermodynamic stability of previously unmeasured G-quadruplexes from sequence information alone.[43] The algorithm relied primarily on experimentally measured T_m values for a quadruplex training set, a perfectly reasonable starting point but a rather primitive measure of stability nonetheless. Such predictive algorithms could be greatly improved by use of more complete and more accurate thermodynamic parameters obtained from more realistic models of the denaturation process.

Support for Sequential Unfolding Mechanism. A useful aspect of using SVD to analyze multiwavelength data sets is that it provides an estimation of the relative contribution of each species to the temperature profile. All spectrally visible species contribute to the overall signal as a function of temperature and wavelength according to the magnitude of their respective singular values. Thus the melting profile of each species during the melt can be visualized by plotting the magnitude of the corresponding **V** vector as a function of temperature. **V** profiles that vary in a nonrandom manner with temperature can be assigned to individual spectroscopic species in a model-independent manner. A quantitative means of establishing whether a particular **V** profile varies periodically or randomly is to calculate the autocorrelation coefficient of the successive elements of the **V** vector. When this test of all the data sets in this study was carried out over the complete temperature range, the **V** vectors for all (except one) had autocorrelation coefficients ≥0.75 for the three **V** vectors with the highest S value, indicating a high degree of correlation for these vectors. The remaining vectors have autocorrelation coefficients <0.75 (see Supporting Information). The exception is the data set for 6-Fam-Tel22-Tamra which by this criterion has four significant **V** vectors. However, the T_m associated with $\mathbf{V}_4$ is ∼86 °C; this high temperature reflects a process that occurs postmelting of the intermediate species. Since none of the other constructs exhibited such a high T_m species, it seems likely that this process is associated with the donor−acceptor pair rather than quadruplex unfolding *per se*.

A criterion for distinguishing among models with differing numbers of adjustable parameters (such as model 4 from 5) is the AIC value. For all of the data sets, there was generally improvement in AIC when additional steps were included. However, it was not always possible to distinguish between models with the same number of steps because these models gave approximately the same AIC. Although including an additional step in the model generally gave improved fits, we excluded models that had **V** vector autocorrelations <0.75 since this would indicate temperature variation in the amplitude vector that was inconsistent with the variation expected for a melting phenomenon. Because the autocorrelation coefficients of $\mathbf{V}_4$ for the 2-AP data sets did not meet this criterion, the data were fit to the two-step model 3.

Three-step models 4 and 5 gave equivalent fits to the data sets in terms of the χ^2 and AIC criteria. We prefer the three-step sequential model for the following reasons. First, both Tel22 and 2GKU gave equally good fits to this model, even though Tel22 in KCl is known to consist of at least two conformers in approximately equal amounts (e.g., the ΔG of conversion between the two species ≈0), while 2GKU is >90% a single conformer. The F state likely consists of an ensemble of closely related, nearly isoenergetic conformations that convert to the I states and then to the U ensemble rather than states F_1 and F_2 unfolding to the U state without passing through an intermediate state that is present in a detectable concentration.

Fluorescence Emission Spectra of the Thermal Intermediates Are Inconsistent with the Properties expected of the parallel fold. Since the A residues located within the TTA loops are in equivalent environments in the symmetrical all-parallel topology, we expect the fluorescence emission properties of the 2-AP analogs to be similar if the thermal intermediate is an all-parallel structure. A similar strategy has been previously used to distinguish the solution structure of Tel22 from the crystal structure; this reference contains a detailed structural justification for the assertion of topological equivalence of the loop adenine residues in the all-parallel structure.[35] Figure 5A−C compares the calculated emission spectra for the F and thermally unfolded U ensembles of the four 2-AP derivatives of Tel22 in 25 mM KCl. The spectra are similar to those previously published.[35] Figure 5B depicts the emission spectra deduced for the I state in the

thermally induced unfolding of the Tel22 derivatives. Comparison of the spectra in Figure 5A−C shows two features: First, the quantum yield is larger for 2-AP emission at all positions when compared to the corresponding F and U states. Second, the quantum yield is nearly the same for 2-AP in positions 1 and 7, suggesting that these residues experience fewer stacking interactions with other residues of the folded structure. In other words, these residues, both of which are located in the first arm of the folded quadruplex, experience more freedom of motion in the intermediate than in either the folded or unfolded states.

The emission spectrum of 6-FAM-Tel22-Tamra in the I state is also inconsistent with that expected for the parallel conformation. The intermediate spectrum in Figure 6D shows a decrease in the FRET efficiency compared to the unfolded state. The decreased FRET efficiency is not as strong as that for the U state, implying that I retains structure but that the distance between donor and acceptor and/or their relative orientations is significantly altered compared to both the F and U ensembles. Examination of a molecular model of Tel22 in the parallel conformation shows that the 5′ and 3′ ends of the molecule, where the donor and acceptor are attached, are relatively close together (6.9 Å calculated from the crystal structure).[44] Thus there should be significant donor to acceptor energy transfer which was not observed. In fact, the degree of end-to-end separation is nearly as great as for the fully unfolded state.

Thermal Intermediate May Be a Triplex. Several groups have suggested that cation-driven quadruplex folding may proceed through a hairpin duplex that in a stepwise manner adds consecutive strands to form a triplex intermediate consisting of three stacks of three H-bonded G residues, followed by association of the fourth G_3 run to form the nascent quadruplex.[45−49] Subsequent slow relaxations result in positioning the loops with respect to the G-stack and adjustment of the loop topology to ultimately form the thermodynamically most stable structure(s). For a quadruplex with four G_3 runs such as those in this study, either the first or fourth G_3 run could be added last; thus, there could be two triplex structures depending on which run was added last.

Until recently, this folding pathway was speculative. However, Mashimo et al.[14] published a rigorous molecular dynamics analysis of these pathways and thereby provided a detailed visualization and energetic analysis of the triplex folding pathway that suggested that triplex structures are energetically feasible, i.e., G-triplets were nearly as stable as G-quartets (−50.6 vs −67.8 kcal mol^{-1} G). More recently, Koirala et al.,[40] building on previous studies by others, investigated the structure of d[TTA(GGGTTA)$_3$] (Tel-3G), a sequence that contains three tandem G_3 repeats. Based on physical studies (optical tweezers and CD), molecular dynamics and footprinting, they demonstrated that in the presence of 100 mM NaCl, this sequence forms a triplex structure. The published CD spectrum of the triplex in NaCl is similar to the shape of the CD spectrum of the 55−60 °C intermediate observed in our studies. This similarity, as well as the fluorescence properties of the corresponding melting intermediate observed in this study, suggests the possibility that it is a mixture of triplex states of the human telomeric DNA oligonucleotide.

Comparison with Calorimetry. A melting intermediate was previously identified for the denaturation of the human telomere quadruplex (TTAGGG)$_4$ by a combined CD and DSC study.[12] A very recent calorimetric/CD study used a sophisticated global analysis method obtained the thermodynamic parameters for the denaturation of the human telomere quadruplex AGGG(TTAGGG)$_3$ in K^+ solutions.[13] A single intermediate was identified, corresponding to our mechanism 3 (Scheme 1). Our data suggest an additional intermediate is necessary. Our results complement and extend this recent study and fully agree about the need to include intermediate states along the denaturation pathway, a conclusion arrived at by independent physical methods. There is also agreement that one intermediate state may be a triplex form. The strength and novelty of our approach are that the spectroscopic properties of the intermediates are defined, providing a deeper characterization of their physical properties.

An important difference between the CD/DSC study and ours is that Bončina et al.[13] were able to determine a heat capacity change (ΔC_p) for quadruplex unfolding, which we are not able to do with confidence. ΔC_p values are best determined by calorimetry[50,51] and are notoriously difficult to obtain from fits of spectroscopic thermal denaturation data alone without more elaborate protocols that combine chemical and thermal denaturation experiments.[52,53] Inclusion of ΔC_p values in our analysis would introduce many additional parameters that would tax our nonlinear fitting methods. However, we can estimate the consequences of neglecting ΔC_p values on some of our parameters. Bončina and co-workers report an overall ΔC_p value of 310 cal mol^{-1} K^{-1} for the unfolding of the human telomere quadruplex in K^+ solution. (A much larger calorimetric value of ≈1600 cal mol^{-1} K^{-1} was reported for the unfolding of the same quadruplex in Na^+ solution,[54] a value that seems unreasonably large but which attests to the difficulty of obtaining accurate ΔC_p values even by calorimetry.) For the final step in the unfolding process, Bončina and co-workers report an enthalpy value of 28.8 kcal mol^{-1} at 25 °C compared to our value for a similar step of 45.3 kcal mol^{-1} at 61.4 °C. If we correct our value using the reported ΔC_p value, we estimate an enthalpy of 33.3 kcal mol^{-1} at 25 °C, in good agreement (within about 15%) with the calorimetric value. For the first step in the unfolding process, a negligible heat capacity change was reported. The reported enthalpy change of 26.7 ± 1.0 kcal mol^{-1} at 25 °C is in good agreement with our value of 21.9 ± 4.7 kcal mol^{-1} at 35.2 °C, although the calorimetrically determined value is clearly more precise. Where comparison is possible, the values obtained in our study agree well with the results of Bončina and co-workers. Neglect of ΔC_p would lead to an overestimate of the magnitudes of our free energy changes at 20 °C (Table 4). If we assume the ΔC_p of Bončina and co-workers, our estimate of ΔG_{Total} would decrease from −9.5 to −8.3 kcal mol^{-1}. A variety of calorimetric studies is underway in our laboratory to address the issue of heat capacity changes, but these are incomplete and beyond the scope of this report.

One reviewer questioned if neglect of heat capacity changes might have influenced our choice of the most probable mechanism and suggested that if ΔC_p parameters were included we might choose the three-state model (mechanism 3, Scheme 1) over the four-state model (mechanism 4, Scheme 1). That is not likely to be the case. A key element in our selection of a mechanism comes from SVD analysis which enumerates in a model-independent fashion the number of significant spectral species that must be accounted for. There is little ambiguity in the SVD analysis of CD data for Tel22 (Table 2) that four species are needed, as was subsequently confirmed by the statistical comparison of fitting models (Table 3). The model-

free SVD analysis places valuable limits on the minimal number of species that must be include in any mechanism, four in this case.

CONCLUSIONS

Our data show that thermal denaturation of the human telomere quadruplex is not a simple two-state process but rather proceeds along a sequential pathway with multiple populated intermediate states. One of these states is most probably a triple helical form, as proposed by recent molecular dynamics simulations.

ASSOCIATED CONTENT

Supporting Information

Equations for fitting thermal unfolding data for mechanisms 1−5 in Scheme 1; spectral data; SVD analysis; and fitting statistics for thermal unfolding data of the 2AP derivatives of Tel22 and of oligonucleotides 2GKU, 2AQY, and Tel-3G. This information is available free of charge via the Internet at http://pubs.acs.org.

AUTHOR INFORMATION

Corresponding Author

j.chaires@lousivlle.edu

Notes

The authors declare no competing financial interest.

ACKNOWLEDGMENTS

Supported by grant CA35635 from the National Cancer Institute and by the James Graham Brown Foundation.

REFERENCES

(1) Chan, S. R. W. L.; Blackburn, E. H. *Philos. Trans. R. Soc., B* **2004**, *359*, 109.
(2) Moyzis, R. K.; Buckingham, J. M.; Cram, L. S.; Dani, M.; Deaven, L. L.; Jones, M. D.; Meyne, J.; Ratliff, R. L.; Wu, J. R. *Proc. Natl. Acad. Sci. U.S.A.* **1988**, *85*, 6622.
(3) Cross, S. H.; Allshire, R. C.; McKay, S. J.; McGill, N. I.; Cooke, H. J. *Nature* **1989**, *338*, 771.
(4) Wright, W. E.; Tesmer, V. M.; Huffman, K. E.; Levene, S. D.; Shay, J. W. *Genes Dev.* **1997**, *11*, 2801.
(5) Shay, J. W.; Wright, W. E. *Sem. Cancer Biol.* **2011**, *21*, 349.
(6) Burge, S.; Parkinson, G. N.; Hazel, P.; Todd, A. K.; Neidle, S. *Nucleic Acids Res.* **2006**, *34*, 5402.
(7) Mergny, J. L.; Phan, A. T.; Lacroix, L. *FEBS Lett.* **1998**, *435*, 74.
(8) Mergny, J. L.; Lacroix, L. *Oligonucleotides* **2003**, *13*, 515.
(9) Mergny, J. L.; Lacroix, L. *Current Protocols in Nucleic Acid Chemistry*; John Wiley & Sons, Inc.: Hoboken, NJ, 2009; Chpt 17, Unit 17 1.
(10) Lane, A. N.; Chaires, J. B.; Gray, R. D.; Trent, J. O. *Nucleic Acids Res.* **2008**, *36*, 5482.
(11) Chaires, J. B. *FEBS J.* **2010**, *277*, 1098.
(12) Antonacci, C.; Chaires, J. B.; Sheardy, R. D. *Biochemistry* **2007**, *46*, 4654.
(13) Bončina, M.; Lah, J.; Prislan, I.; Vesnaver, G. *J. Am. Chem. Soc.* **2012**, *134*, 9657.
(14) Mashimo, T.; Yagi, H.; Sannohe, Y.; Rajendran, A.; Sugiyama, H. *J. Am. Chem. Soc.* **2010**, *132*, 14910.
(15) Gray, R. D.; Chaires, J. B. *Current Protocols in Nucleic Acid Chemistry*; John Wiley & Sons, Inc.: Hoboken, NJ, 2011; Chapter 17, Unit17 4.
(16) Dignam, J. D.; Qu, X.; Chaires, J. B. *J. Biol. Chem.* **2001**, *276*, 4028.
(17) Greenfield, N. J. *Nat. Protoc.* **2006**, *1*, 2527.
(18) Saroff, H. A. *Anal. Biochem.* **1989**, *176*, 161.
(19) Motulsky, H.; Christopoulos, A. *Fitting Models to Biological Data Using Linear and Nonlinear Regression*; GraphPad Software Inc.: San Diego, CA, 2003.
(20) Phan, A. T.; Patel, D. J. *J. Am. Chem. Soc.* **2003**, *125*, 15021.
(21) Ambrus, A.; Chen, D.; Dai, J.; Bialis, T.; Jones, R. A.; Yang, D. *Nucleic Acids Res.* **2006**, *34*, 2723.
(22) Gray, R. D.; Petraccone, L.; Trent, J. O.; Chaires, J. B. *Biochemistry* **2010**, *49*, 179.
(23) Lumry, R.; Biltonen, R. *Biopolymers* **1966**, *4*, 917.
(24) Wallimann, P.; Kennedy, R. J.; Miller, J. S.; Shalongo, W.; Kemp, D. S. *J. Am. Chem. Soc.* **2003**, *125*, 1203.
(25) Henry, R.; Hofrichter, J. In *Methods in Enzymology*; Brand, L., Johnson, M., Eds.; Academic Press: New York, 1992; Vol. *210*, p 129.
(26) Singh, V.; Azarkh, M.; Exner, T. E.; Hartig, J. S.; Drescher, M. *Angew. Chem., Int. Ed.* **2009**, *48*, 9728.
(27) Karsisiotis, A. I.; Hessari, N. M.; Novellino, E.; Spada, G. P.; Randazzo, A.; Webba da Silva, M. *Angew. Chem., Int. Ed.* **2011**, *50*, 10645.
(28) Miller, M. C.; Buscaglia, R.; Chaires, J. B.; Lane, A. N.; Trent, J. O. *J. Am. Chem. Soc.* **2010**, *132*, 17105.
(29) Jean, J. M.; Hall, K. B. *Proc. Natl. Acad. Sci. U.S.A.* **2001**, *98*, 37.
(30) Rachofsky, E. L.; Osman, R.; Ross, J. B. A. *Biochemistry* **2001**, *40*, 946.
(31) O'Neill, M. A.; Barton, J. K. *J. Am. Chem. Soc.* **2002**, *124*, 13053.
(32) Jean, J. M.; Krueger, B. P. *J. Phys. Chem. B* **2006**, *110*, 2899.
(33) Gray, R. D.; Petraccone, L.; Buscaglia, R.; Chaires, J. B. *Methods Mol. Biol.* **2010**, *608*, 121.
(34) Buscaglia, R.; Jameson, D. M.; Chaires, J. B. *Nucleic Acids Res.* **2012**, *40*, 4203.
(35) Li, J.; Correia, J. J.; Wang, L.; Trent, J. O.; Chaires, J. B. *Nucleic Acids Res.* **2005**, *33*, 4649.
(36) Juskowiak, B. *Anal. Chim. Acta* **2006**, *568*, 171.
(37) Juskowiak, B.; Takenaka, S. *Methods Mol. Biol.* **2006**, *335*, 311.
(38) Luu, K. N.; Phan, A. T.; Kuryavyi, V.; Lacroix, L.; Patel, D. J. *J. Am. Chem. Soc.* **2006**, *128*, 9963.
(39) Zhang, N.; Phan, A. T.; Patel, D. J. *J. Am. Chem. Soc.* **2005**, *127*, 17277.
(40) Koirala, D.; Mashimo, T.; Sannohe, Y.; Yu, Z.; Mao, H.; Sugiyama, H. *Chem. Commun. (Cambridge, U. K.)* **2012**, *48*, 2006.
(41) Ginsburg, A.; Carroll, W. R. *Biochemistry* **1965**, *4*, 2159.
(42) Haq, I.; Chowdhry, B. Z.; Chaires, J. B. *Eur. Biophys. J.* **1997**, *26*, 419.
(43) Stegle, O.; Payet, L.; Mergny, J. L.; MacKay, D. J.; Leon, J. H. *Bioinformatics* **2009**, *25*, i374.
(44) Parkinson, G. N.; Lee, M. P.; Neidle, S. *Nature* **2002**, *417*, 876.
(45) Mashimo, T.; Sannohe, Y.; Yagi, H.; Sugiyama, H. *Nucleic Acids Symp. Ser.* **2008**, 409.
(46) Dai, J.; Carver, M.; Yang, D. *Biochimie* **2008**, *8*, 1172.
(47) Gray, R. D.; Li, J.; Chaires, J. B. *J. Phys. Chem. B* **2009**, *113*, 2676.
(48) Su, D. G.; Fang, H.; Gross, M. L.; Taylor, J. S. *Proc. Natl. Acad. Sci. U. S. A.* **2009**, *106*, 12861.
(49) Zhang, Z.; Dai, J.; Veliath, E.; Jones, R. A.; Yang, D. *Nucleic Acids Res.* **2010**, *38*, 1009.
(50) Privalov, P. L.; Khechinashvili, N. N. *J. Mol. Biol.* **1974**, *86*, 665.
(51) Becktel, W. J.; Schellman, J. A. *Biopolymers* **1987**, *26*, 1859.
(52) Pace, C. N.; Laurents, D. V. *Biochemistry* **1989**, *28*, 2520.
(53) Talla-Singh, D.; Stites, W. E. *Proteins* **2008**, *71*, 1607.
(54) Majhi, P. R.; Qi, J.; Tang, C. F.; Shafer, R. H. *Biopolymers* **2008**, *89*, 302.